Special Issue Article

Advances in Mechanical Engineering

Advances in Mechanical Engineering
2017, Vol. 9(2) 1–11

DOI: 10.1177/1687814016689039
journals.sagepub.com/home/ade
SAGE

Pitching axis control for a satellite camera based on a novel active disturbance rejection controller

Bingyou Liu[1,2], Yi Jin[1], Changan Zhu[1] and Changzheng Chen[3]

Abstract

The pitching axis of a satellite camera is controlled under the weightless environment. A novel active disturbance rejection controller is designed to eliminate the influences of the pitching axis. The novel active disturbance rejection controller is designed based on a new nonlinear function, and thus, this function is first established. The function exhibits better continuity and smoothness than previously available functions, hence, it can effectively improve the high-frequency flutter phenomenon. Therefore, the novel active disturbance rejection controller based on the new nonlinear function can eliminate disturbances of the pitching axis. The novel active disturbance rejection controller is composed of a tracking differentiator, a novel extended state observer, and a novel nonlinear state error feedback. The tracking differentiator is used to arrange the transient process. Nonlinear dynamics, model uncertainty, and external disturbances are extended to a new state. The novel extended state observer is utilized to observe this state. The overtime variation of the system can be predicted and compensated using the novel extended state observer. The novel nonlinear state error feedback is adopted to restrain the residual errors of the system. Finally, simulation experiments are performed, and results show that the novel active disturbance rejection controller exhibits better performance than the traditional active disturbance rejection controller.

Keywords

Novel active disturbance rejection controller, pitching axis, speed control, satellite camera, nonlinear function

Date received: 12 April 2016; accepted: 14 December 2016

Academic Editor: Ramoshweu Lebelo

Introduction

The posture of satellite cameras is controlled by three axes. The pitch posture is controlled by the pitching axis, the side swing posture by the side swing axis, and the drift angle by the drift angle adjustment axis. Pitching axis is important for the posture control system of satellite cameras. A three-loop (i.e. current loop, speed loop, and position loop) servo control system is adopted as the control strategy for the pitching axis control system. The speed loop of the pitching axis should be controlled in real time to enable it to achieve good performance. Guan and Zheng[1] and Yang et al.[2] introduced an integrated design method for posture control in satellite cameras. Wang et al.[3] presented an on-orbit calibration approach for satellite cameras based on an iteration method with weights. However, these works did not provide an effective method to eliminate disturbances in the speed-loop control system

[1]Department of Precision Machinery & Instrumentation, University of Science and Technology of China, Hefei, China
[2]Key Lab of Electric and Control of Anhui Province, Anhui Polytechnic University, Wuhu, China
[3]Changchun Institute of Optics, Fine Mechanics and Physics, Chinese Academy of Sciences, Changchun, China

Corresponding author:
Yi Jin, Department of Precision Machinery & Instrumentation, University of Science and Technology of China, Hefei 230027, China.
Email: jinyi08@ustc.edu.cn

of satellite cameras. In this study, a novel active disturbance rejection controller (ADRC) is used in the speed-loop control system to enable it to achieve good performance.

The ADRC was introduced by Han.[4] This controller does not depend on the system model, and instead, it is a control method that relies on the errors of the process to eliminate system errors.[5,6] The ADRC is composed of a tracking differentiator (TD), an extended state observer (ESO), and a nonlinear state error feedback (NLSEF). The TD is used to arrange the transient process. The ESO is utilized to estimate the total disturbances of the system. The NLSEF is adopted to confine residual errors in the system.[7–9] Extensive research on the application of ADRC has been conducted locally and internationally, and several achievements have been reported. For example, Chong et al.[10] and Guo and collegues[11–13] designed a fuzzy ADRC and improved the performance of a system. However, the accurate estimation and real-time compensation of the total disturbance were not discussed in detail. Fu et al.,[14] Xia et al.,[15] Sira-Ramírez et al.,[16] and Zhu et al.[17] studied a control system based on ADRC. However, the parameters of ADRCs were too extensive to establish, and thus, they did not provide specific rules for doing so. A novel, unifying concept of disturbance rejector is proposed to compliment the traditional notion of controller.[18] The methodology of ADRC and the progress of its theoretical analysis are reviewed.[19] Wang et al.[20] designed an ESO with a power function filter to effectively estimate the state variables of a system. However, the amount of noise was substantial when the differential was estimated. Wu and Chen[21] and Lin et al.[22] regarded the inertia filtering function as a known part of a system, and thus, the number of parameters that should be set was reduced. Nevertheless, noise was still not eliminated in this system because the power function was used in ADRC. In another study, an ADRC was adopted to analyze the stabilization of nonlinear systems with actuator saturation.[23] Meanwhile, another work applied an ADRC with an adaptive ESO in the air–fuel ratio control of gasoline engines.[24] In addition, the absolute stability of nonlinear ADRC for single-input and single-output (SISO) systems was analyzed using the circle criterion method.[25] Moreover, the trajectory tracking problem of a delta robot was solved through an adaptive ADRC.[26] However, the ADRCs used in the aforementioned works were traditional and designed based on a nonlinear function called f_{non2}. The traditional ADRC cannot effectively eliminate the high-frequency flutter of a system because the nonlinear function is ideal, and although the function is continuous, it is non-derivable. Therefore, designing a novel ADRC is crucial to eliminate the high-frequency flutter of the system.

In this study, a novel ADRC is designed based on a new nonlinear function called f_{nonnew}. The structure chart of the pitching axis is presented, and the mathematical model for the actuator is calculated. Then, the nonlinear function f_{non2} is improved to a new nonlinear function f_{nonnew}, which is continuous and derivable. A novel ADRC based on the new nonlinear function f_{nonnew} for the pitching axis of satellite cameras is established. Simulations are conducted in the pitching axis control system for cases that adopt the traditional ADRC and novel ADRC. The simulation results are discussed in this section.

Structure chart and model

Structure chart of the pitching axis

The structure chart of the pitching axis is shown in Figure 1. The rotating mechanism is fixed on the satellite using a holder. The satellite camera is fixed on the pitching axis, therefore, the pitching posture control for the pitching axis can be realized. A balance wheel is used to balance the angular momentum caused by the pitching movement. A reducer, a sun gear, and a planet gear are used as transmissions to control the angular velocity of the balance wheel.

Permanent magnet synchronous motor models

In this study, a permanent magnet synchronous motor (PMSM) is used as the actuator in the pitching axis control system. Therefore, PMSM models are established in this study. These models include a voltage equation, a flux equation, a torque equation, and a kinematic equation. The following assumptions are made. First, the saturation effects of the iron core are disregarded. Second, the air-gap magnetic field exhibits a normal distribution. Third, the wastage of the eddy current and the magnetic field is disregarded. Fourth, no damper winding exists on the motor rotor. The kinematic equation for the PMSM on the two-phase system (i.e. *dq* coordinate system) is given as follows

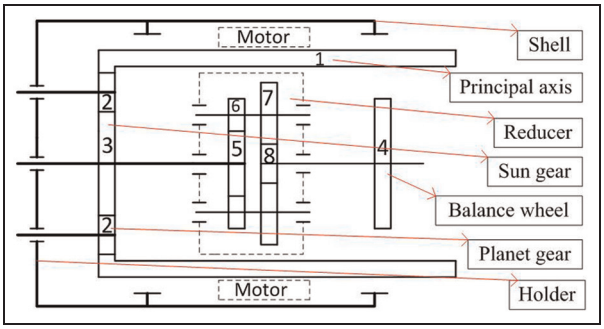

Figure 1. Structure chart of the pitching axis.

$$\dot{\omega} = \frac{1}{J}(T_e - T_L - B\omega) \tag{1}$$

where B is the friction coefficient, J is the rotational inertia of the motor, ω is the angular speed of the motor rotor, T_e is the electromagnetic torque of the motor, and T_L is the load torque of the motor.

Design of novel ADRC

Improvement of nonlinear function

The improvements of nonlinear function follow the succeeding forms based on extensive discussions regarding the simulation. First, the nonlinear function was selected as the $f_{non1}(\cdot)$ function. The expression and curves of $f_{non1}(\cdot)$ function when $\alpha = 0,\ 0.25,\ 0.5,\ and\ 1$ are shown as follows (Figure 2)

$$f_{non1}(e,\alpha) = |e|^{\alpha} sign(e) \tag{2}$$

The derivation of function $f_{non1}(\cdot)$ on the origin of the coordinates approaches to infinity based on the expression and curves of the $f_{non1}(\cdot)$ function. Thus, the function $f_{non1}(\cdot)$ will cause the high-frequency flutter phenomenon around the origin of the coordinates. Consequently, the nonlinear function $f_{non1}(\cdot)$ is improved to function $f_{non2}(\cdot)$. The expression of function $f_{non2}(\cdot)$ is given as follows

$$f_{non2}(e,\alpha,\delta) = \begin{cases} |e|^{\alpha} sign(e), & |e| > \delta \\ \frac{e}{\delta^{1-\alpha}}, & |e| \le \delta \end{cases}, \delta > 0 \tag{3}$$

The characteristics of function $f_{non2}(\cdot)$ are expressed as follows. The value of α influences the degree of nonlinearity of the function $f_{non2}(\cdot)$. The value of α is set between 0 and 1 based on experience. When $\alpha = 0$, the degree of nonlinearity of the function $f_{non2}(\cdot)$ is the most serious. When $\alpha = 1$, the degree of linearity of the function $f_{non2}(\cdot)$ is optimal. The value of δ is the linear interval width of the function $f_{non2}(\cdot)$, which is related to the error range of the system. In practical applications, the value of δ is generally set to $\delta = 0.01$. When the input is an error signal, the system can rapidly achieve stability by adjusting the parameter values of the function $f_{non2}(\cdot)$. Although the function $f_{non2}(\cdot)$ is continuous, it is non-derivable. If the value of δ is too small, the $f_{non2}(\cdot)$ function will produce high-frequency flutter phenomenon. Adjusting the value of δ is difficult because the control performance of the function $f_{non2}(\cdot)$ is sensitive to the value of δ. Thus, the nonlinear function is improved to $f_{nonnew}(\cdot)$ function. The $f_{nonnew}(\cdot)$ function is a continuous and derivable nonlinear function, which is expressed as follows[27,28]

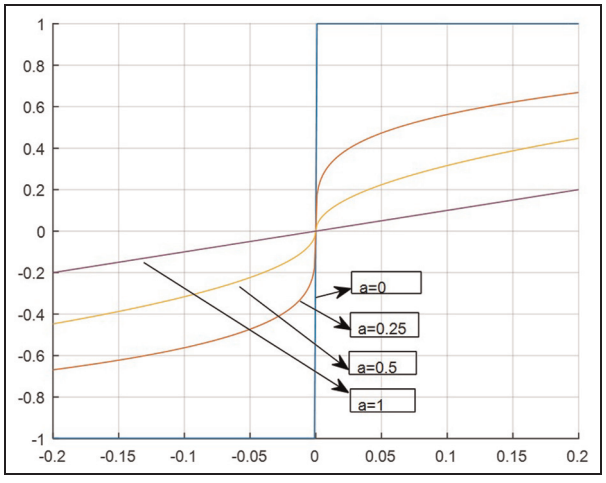

Figure 2. Characteristic curves of $f_{non1}(\cdot)$ function when $\alpha = 0,\ 0.25,\ 0.5,\ and\ 1$.

$$f_{nonnew}(\cdot) = \begin{cases} |e|^{\alpha} sign(e), & |e| > \delta > 0 \\ \rho_1 e + \rho_2 e^2 + \rho_3 \sin e, & |e| \le \delta, \delta > 0 \end{cases} \tag{4}$$

where ρ_1, ρ_2, ρ_3 are the parameters that need to be determined. The value of δ is set to $\delta < 1$. The expression $f_{nonnew}(\cdot) = 0$ is tenable around the origin of the coordinates because the $f_{nonnew}(\cdot)$ function continuously occurs around this location. The nonlinear function $f_{nonnew}(\cdot)$ should satisfy the following continuous and derivable conditions.

When $e = \delta$, $f_{nonnew}(\cdot) = \delta^{\alpha}$, and $df_{nonnew}(e,\alpha,\delta)/d\delta = \alpha\delta^{\alpha-1}$, therefore, equations (5) and (6) can be obtained as follows

$$\rho_1\delta + \rho_2\delta^2 + \rho_3 \sin\delta = \delta^{\alpha} \tag{5}$$

$$\rho_1 + 2\rho_2\delta + \rho_3 \cos\delta = \alpha\delta^{\alpha-1} \tag{6}$$

When $e = -\delta$, $f_{nonnew}(\cdot) = -\delta^{\alpha}$, and $df_{nonnew}(e,\alpha,\delta)/d\delta = \alpha\delta^{\alpha-1}$, therefore, equations (7) and (8) can be obtained as follows

$$-\rho_1\delta + \rho_2\delta^2 - \rho_3 \sin\delta = -\delta^{\alpha} \tag{7}$$

$$-\rho_1 + 2\rho_2\delta - \rho_3 \cos\delta = \alpha\delta^{\alpha-1} \tag{8}$$

From equations (5)–(8), the following expressions can be derived

$$\rho_1 = \alpha\delta^{\alpha-1} - \frac{(1-\alpha)\delta^{\alpha}\cos\delta}{\sin\delta - \delta\cos\delta} \tag{9}$$

$$\rho_2 = 0 \tag{10}$$

$$\rho_3 = \frac{(1-\alpha)\delta^{\alpha}}{\sin\delta - \delta\cos\delta} \tag{11}$$

Thus, the nonlinear function $f_{nonnew}(\cdot)$ can be expressed as follows

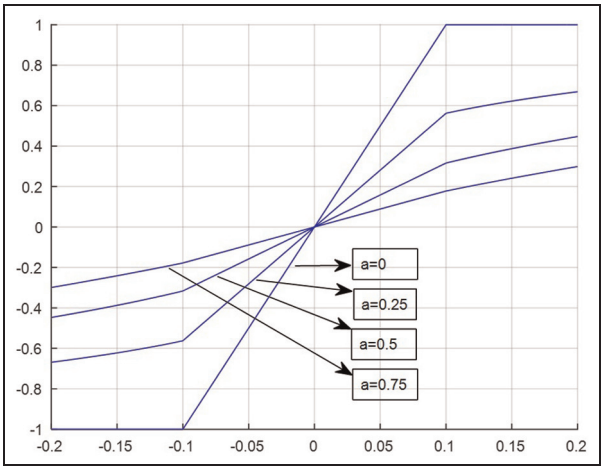

Figure 3. Characteristic curves of $f_{non2}(\cdot)$ when $\delta = 0.1$, $\alpha = 0,\ 0.25,\ 0.5,$ and 0.75.

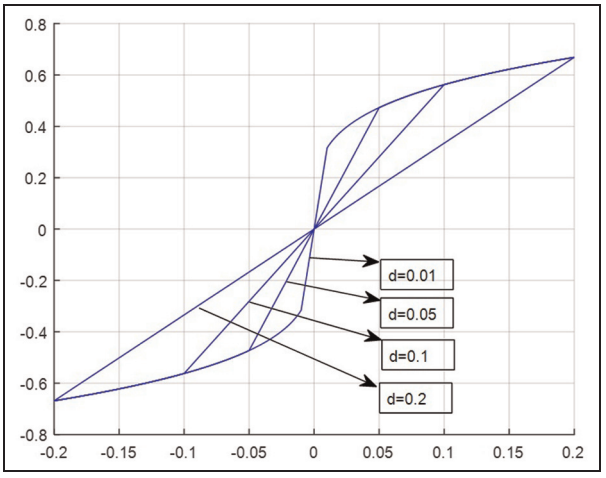

Figure 5. Characteristic curves of $f_{non2}(\cdot)$ when $\alpha = 0.25$, $\delta = 0.01,\ 0.05,\ 0.1,$ and 0.2.

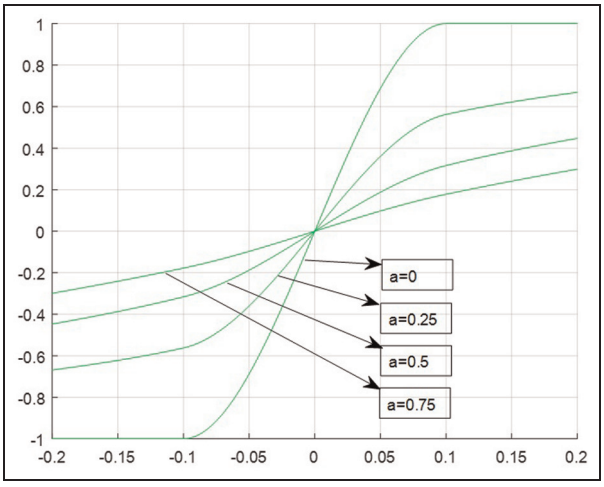

Figure 4. Characteristic curves of $f_{nonnew}(\cdot)$ when $\delta = 0.1$, $\alpha = 0,\ 0.25,\ 0.5,$ and0.75.

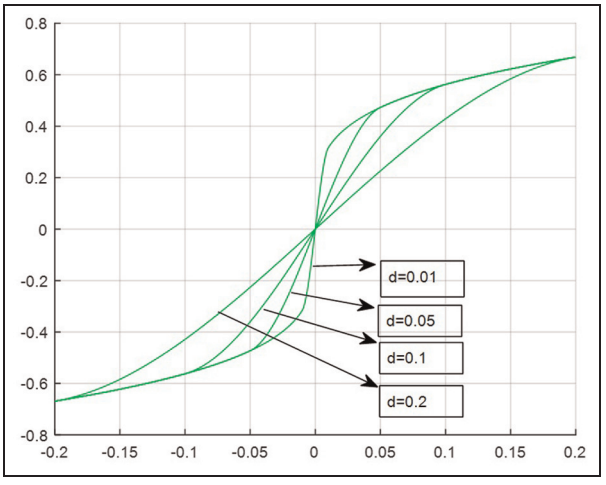

Figure 6. Characteristic curves of $f_{nonnew}(\cdot)$ when $\alpha = 0.25$, $\delta = 0.01,\ 0.05,\ 0.1,$ and0.2.

$$f_{nonnew}(e,\alpha,\delta) = \begin{cases} \left(\alpha\delta^{\alpha-1} - \dfrac{(1-\alpha)\delta^{\alpha}\cos\delta}{\sin\delta - \delta\cos\delta}\right)e + \dfrac{(1-\alpha)\delta^{\alpha}}{\sin\delta - \delta\cos\delta}\sin e, & |e| \le \delta \\ |e|^{\alpha} sign(e), & |e| > \delta \end{cases} \tag{12}$$

The expression of the nonlinear function $f_{nonnew}(\cdot)$ indicates that the coefficient of e^2 is 0. Hence, the nonlinear function $f_{nonnew}(\cdot)$ exhibits better smoothness than the nonlinear functions $f_{non1}(\cdot)$ and $f_{non2}(\cdot)$. Simulations are performed on the three nonlinear functions under the following cases: (1) $\delta = 0.1$, $\alpha = 0,\ 0.25,\ 0.5,$ and 0.75; (2) $\alpha = 0.25$, $\delta = 0.01,\ 0.05,\ 0.1,$ *and* 0.2. The simulation results are shown in Figures 3–7.

The simulation results demonstrate that the $f_{nonnew}(\cdot)$ function exhibits better continuity and derivability than

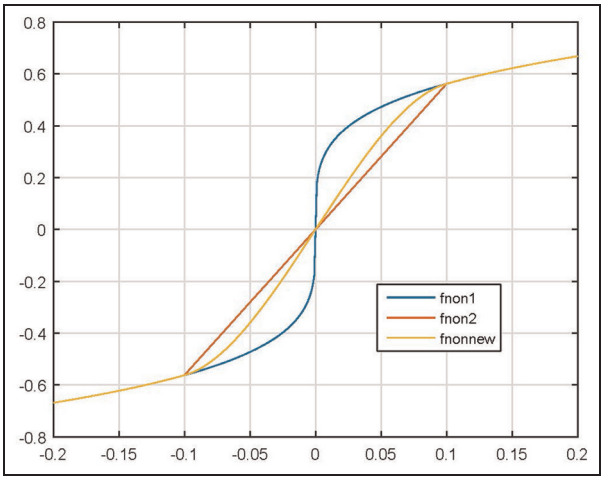

Figure 7. Characteristic curves of $f_{non1}(\cdot)$, $f_{non2}(\cdot)$, and $f_{nonnew}(\cdot)$ when $\alpha = 0.25$ and $\delta = 0.1$.

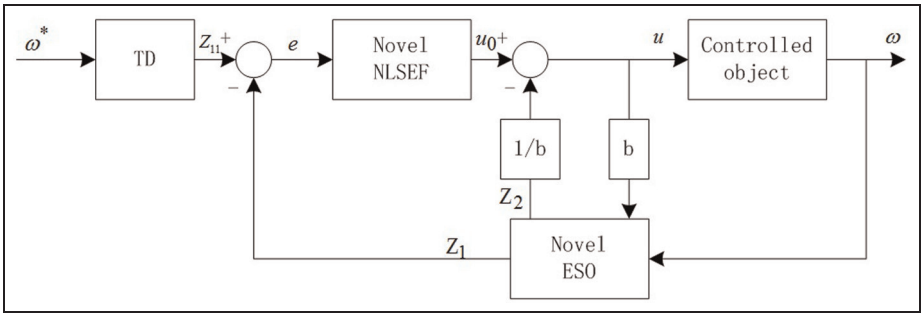

Figure 8. Control principle diagram of the speed loop based on novel ADRC.

functions $f_{non1}(\cdot)$ and $f_{non2}(\cdot)$. Thus, the $f_{nonnew}(\cdot)$ function is insensitive to the selection of the δ value and can avoid the high-frequency flutter phenomenon. In this study, the design of the novel ADRC is based on the $f_{nonnew}(\cdot)$ function.

Novel ADRC design

The key to speed-loop control is controlling the electromagnetic torque. The feedback control can be designed based on the error of the given speed and the speed readings; thus, effective control can be achieved.[29] The control principle diagram of the speed loop based on the novel ADRC is shown in Figure 8.

TD. In the novel ADRC, the TD is used to arrange the transient process. A continuous and differentiable input signal can be obtained using the TD. Thus, drastic changes in the control signal can be effectively avoided. The expression of the TD is given as

$$\begin{cases} fh = f_{ocs}(Z_{11} - y^*, v_2, r_0, h) \\ \dot{Z}_{11} = v_2 \\ \dot{v}_2 = fh \end{cases} \tag{13}$$

where y^* is the output of the system, Z_{11} is the tracking signal of y^*, and r_0 andh_0 are used to establish the speed of the transient process.[30] $f_{ocs}(x_1, x_2, r, h_0)$ is an optimal control synthesis function that can be defined as follows

$$f_{ocs}(v_1, v_2, r, h_0) = -\begin{cases} r\,sign(\alpha), & |\alpha| > \delta \\ r\frac{\alpha}{\delta}, & |\alpha| \le \delta \end{cases} \tag{14}$$

where $\alpha = \begin{cases} v_2 + ((\alpha_0 - \delta)/2)sign(y), & |y| > \delta_0 \\ v_2 + (y/h), & |y| \le \delta_0 \end{cases}$,

$\begin{cases} \delta = rh_0 \\ \delta_0 = \delta h_0 \\ y = v_1 + h_0 v_2 \\ \alpha_0 = \sqrt{\delta^2 + 8r|y|} \end{cases}$, h is the integration step that is set to $h = 0.01$, r is the velocity factor, h_0 is the filter factor, $v(t)$ is the input, and v_1 is the output of the TD. v_1 can track $v(t)$ as fast as possible when the acceleration constraint is $|\ddot{v}| \le r$. When the value of r is high, the tracking speed is fast. v_2 is the differentiation of $v(t)$ when v_1 tracks $v(t)$. h_0 is used to filter the high-frequency interferences of $v(t)$. When the value of h_0 is high, the filtering effect is good.

Novel ESO. The novel ESO is design based on the new nonlinear function $f_{nonnew}(\cdot)$ and is the core of the novel ADRC. Nonlinear dynamics, model uncertainty, and external disturbances are extended to a new state and observed by the novel ESO. The variation of the system over time can be predicted and compensated using the novel ESO. Thus, the robustness of the system can be improved significantly. The general form of the novel ESO is presented as follows. A nonlinear SISO system with unknown disturbances is expressed as

$$x^{(n)} = f\left(x, \ldots, x^{(n-1)}, t\right) + w(t) + bu(t) \tag{15}$$

where $f(x, \ldots, x^{(n-1)}, t)$ is an unknown function comprised by the system state variables, $w(t)$ is the unknown external disturbances of the system, $u(t)$ is the input, $x, \ldots, x^{(n-1)}$ are the state variables of the system, and $x(t)$ is measurable.

Assume that $x_1 = x(t)$, $x_2 = x'(t)$, $\ldots$, $x_n = x^{(n-1)}(t)$. The state space of the system (15) can be expressed as follows

$$\begin{cases} \dot{x}_1 = x_2 \\ \dot{x}_2 = x_3 \\ \vdots \\ \dot{x}_n = f(x_1, x_2, \ldots, x_n) + w(t) + bu(t) \end{cases} \tag{16}$$

Assume that $a(t) = f(x, x^{(1)}, \ldots, x^{(n-1)}, t) + w(t)$. The expression of the novel ESO can be expressed as follows

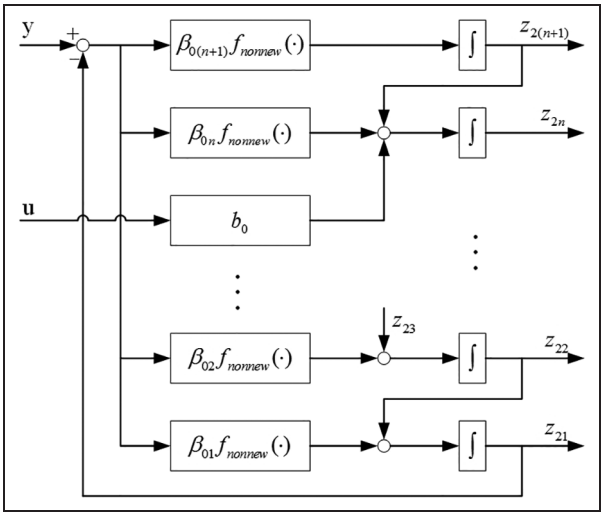

Figure 9. Internal principle diagram of the novel ESO.

$$\begin{cases} e_1 = z_{21} - y \\ \dot{z}_{21} = z_{22} - \beta_{01} f_{nonnew}(e_1, \alpha_{11}, \delta_1) \\ \dot{z}_{22} = z_{23} - \beta_{02} f_{nonnew}(e_1, \alpha_{12}, \delta_1) \\ \vdots \\ \dot{z}_{2n} = z_{2(n+1)} - \beta_{0n} f_{nonnew}(e_1, \alpha_{1n}, \delta_1) + b_0 u(t) \\ \dot{z}_{2(n+1)} = -\beta_{0(n+1)} f_{nonnew}(e_1, \alpha_{1(n+1)}, \delta_1) \end{cases} \tag{17}$$

where $z_{21} \to x(t), \ldots, z_{2n} \to x^{n-1}(t), z_{2(n+1)} \to a(t)$ are the estimations of the unknown functions $f(x, x^{(1)}, \ldots, x^{(n-1)}, t)$ and disturbances $w(t)$. If the nonlinear function $f_{nonnew}(\cdot)$ is selected appropriately, the state variables of the nonlinear system can indicate the state variables of the original system and $a(t)$, respectively. Hence, the novel ESO of the system can be obtained. Furthermore, the uncertain objects and external disturbances in the original system can be compensated using the novel ESO. $\beta_{01}, \beta_{02}, \ldots, \beta_{0n}, \beta_{0(n+1)}$ are the gain coefficients of the novel ESO. b_0 is the estimation of the compensation factor. The internal principle diagram of the novel ESO is presented in Figure 9.

Novel NLSEF. The novel NLSEF is adopted to combine the state variables produced by nonlinearly tracking the TD and the ESO with the error of the estimated value. The expression of the novel NLSEF is given as

$$\begin{cases} e_2 = Z_{11} - Z_{21} \\ u_0 = \beta_1 f_{nonnew}(e_2, \alpha_2, \delta_2) \\ u = \frac{u_0 - Z_{22}}{b_0} \end{cases} \tag{18}$$

where β_1 is the gain coefficient of the novel NLSEF and Z_{22}/b is used to compensate for the internal and external disturbances.

Design of the novel ADRC for a pitching axis

The key to speed-loop control is controlling the electromagnetic torque according to its relationship with the load torque. The feedback control strategy for the speed loop can be designed based on the speed error and the given speed. Therefore, torque control can be effectively achieved. Speed loop is also influenced by uncertain disturbances, such as rotational inertia and load torque. Thus, the main purpose of the speed-loop controller is to eliminate such influences. The disturbances and errors in model linearization are eradicated using the novel ADRC. Hence, the objective of removing uncertain factors is realized. Unknown external disturbances are considered; thus, the input is set to $u = i_q$, whereas the output is set to $y = \omega$. The PMSM kinematic equation can be expressed as follows

$$\dot{\omega} = \frac{3p\varphi_f}{2J} i_q - \frac{B}{J}\omega - \frac{T_L}{J} \tag{19}$$

The novel ADRC of the speed loop can be designed through the following steps. Several definitions are provided as follows

$$x = \omega, \quad a = -\frac{B}{J}, \quad f(x,t) = ax,$$
$$b = 1.5\frac{p\varphi_f}{J}, \quad w(t) = -\frac{T_L}{J}$$

Therefore, the expression of the kinematic equation with extended states can be expressed as follows

$$\begin{cases} \dot{x} = f(x,t) + w(t) + bu \\ y = x \end{cases} \tag{20}$$

Expression of the TD is established as follows

$$\begin{cases} fh = f_{ocs}(Z_{11} - \omega^*, v_2, r_0, h) \\ \dot{Z}_{11} = v_2 \\ \dot{v}_2 = fh \end{cases} \tag{21}$$

Expression of the novel ESO is established as follows

$$\begin{cases} e_1 = Z_{21} - \omega \\ \dot{Z}_{21} = Z_{22} - \beta_{01} f_{nonnew}(e_1, \alpha_0, \delta_1) + b_0 u \\ \dot{Z}_{22} = -\beta_{02} f_{nonnew}(e_1, \alpha_1, \delta_1) \end{cases} \tag{22}$$

Expression of the novel NLSEF is established as follows

$$\begin{cases} e_2 = Z_{11} - Z_{21} \\ u_0 = \beta_1 f_{nonnew}(e_2, \alpha_2, \delta_2) \\ u = \dfrac{u_0 - Z_{22}}{b_0} \end{cases} \tag{23}$$

where ω is the given speed; Z_{21} and Z_{22} are the state variables of the novel ESO; Z_{21} is the tracking signal of the motor speed ω; Z_{22} is the tracking signal of the

Table 1. Parameters of the experiment motor.

Type	Power supply voltage (VAC)	Rated power (W)	Maximum non-loading speed (r/min)	Continuous current (A)	Continuous torque (N m)	Peak current (A)	Peak torque (N m)	Motor pole logarithmic	Resistance (Ω)	Inductance (mH)
KBM-43X01	400	2400	2750	5.1	6.11	18	18	16	2.9	6.8

motor load torque disturbance T_L; β_{01} and β_{02} are the gain coefficients of the novel ESO; α_0 and α_1 are the nonlinear factors that satisfy the condition $0<\alpha_1<\alpha_0\leq 1$, and the values of α_0 and α_1 are set to 1 and0.5,respectively, in this study; δ is a filtering factor with a value of $\delta = 0.01$.

Simulation experiment and discussion

In this section, the novel ADRC is compared with the traditional ADRC to analyze their performances. A PMSM which type is KBM-43X01 was selected as the executing agency of the system. The motor parameters are listed in Table 1. The parameters of the traditional ADRC are provided as follows

$$r = 100,\ h = 0.01,\ \alpha_1 = 0.25,\ \alpha_2 = 0.5,$$
$$\delta_1 = \delta_2 = 0.01,$$
$$\beta_{01} = 100,\ \beta_{02} = 200,\ b_0 = 1,\ \beta_1 = 10$$

The parameters of the novel ADRC are provided as follows

$$r = 100,\ h = 0.01,\ \alpha_1 = 0.25,\ \alpha_2 = 0.5,\ \delta_1 = 0.0001,$$
$$\delta_2 = 0.01,\ \beta_{01} = 100,\ \beta_{02} = 200,\ b_0 = 1,\ \beta_1 = 10$$

Simulations are conducted using the traditional ADRC and the novel ADRC in the following cases. First, simulations are performed when the motor starts without a load. A given speed of 100 r/min is applied on the motor at 0 s. Figure 10 shows the speed response curves under the two control strategies. The figure shows that the novel ADRC has a shorter adjustment time and a smaller overshoot amount than the traditional ADRC. The simulation results demonstrate that the overshoot amount of the novel ADRC is 13.098% less than that of the traditional ADRC, and the response time of the novel ADRC is 1.625 s less than that of the traditional ADRC. The parameters of overshoot amount and response time are presented in Table 2.

Second, simulations are conducted when an external load disturbance is suddenly applied on the motor. The initial speed of the motor is set to 100 r/min. An external load disturbance of 50 r/min is applied on the motor at 5 s. The speed response curves under the two control strategies are shown in Figure 11. The simulation results demonstrate that the novel ADRC has a smaller response curve fluctuation, a shorter recovery time, and a smaller load disturbance influence than the traditional ADRC. The simulation results show that the overshoot amount of the novel ADRC is 13.068% less than that of the traditional ADRC, and its response time is 1.441 s less than that of the traditional ADRC. The speed-loop response parameters are presented in Table 3.

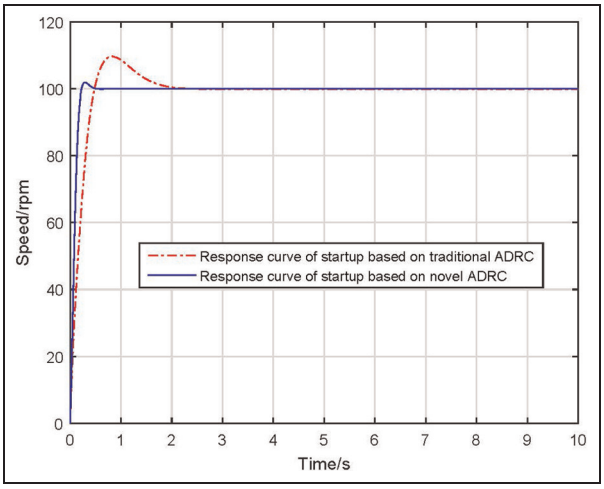

Figure 10. Speed response curve when the motor starts without a load.

Table 2. Response parameters of the system when the motor starts without a load.

Strategy	Overshoot amount (%)	Response time (s)
Traditional ADRC	14.461	2.098
Novel ADRC	1.363	0.473

ADRC: active disturbance rejection controller.

The response curves of output y and state variable Z_{21} with the traditional ADRC are shown in Figure 12.

The response curves of output y and state variable Z_{21} with the novel ADRC are indicated in Figure 13.

As shown in Figures 12 and 13, state variables Z_{21} and Z_{22} can indicate y and dy/dt in real time,

Table 3. Response parameters when an external load disturbance is suddenly applied on the motor.

Strategy	Overshoot amount (%)	Recovery time (s)
Traditional ADRC	14.813	1.773
Novel ADRC	1.745	0.332

ADRC: active disturbance rejection controller.

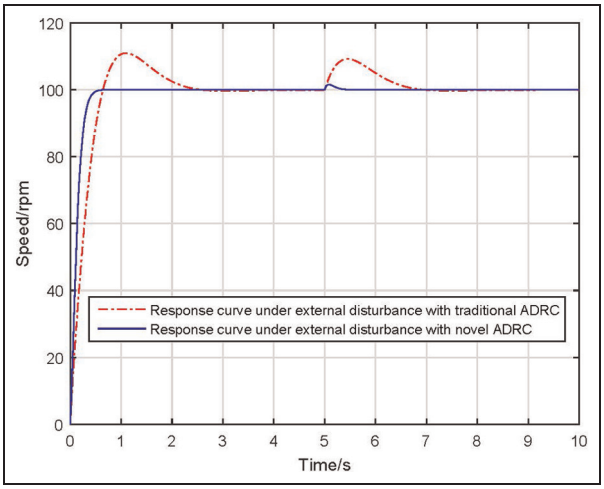

Figure 11. Speed response curve when an external load disturbance is suddenly applied on the motor.

respectively. The novel ADRC and the traditional ADRC both exhibit anti-interference capability. However, the anti-interference capability of the novel ADRC is better than that of the traditional ADRC. The response curves of dy/dt and state variable Z_{22} with the traditional ADRC are shown in Figure 14.

The response curves of dy/dt and state variable Z_{22} with the novel ADRC are presented in Figure 15.

Figure 14 illustrates that dy/dt can precisely identify Z_{22} using the traditional ADRC at 3.321 s. Figure 15 shows that dy/dt can precisely indicate Z_{22} at 0.568 s using the novel ADRC. Thus, the novel ADRC exhibits better indication capability than the traditional ADRC. The response curves for the error of y and Z_{21} are presented in Figure 16.

The response curves for the error of dy/dt and Z_{22} are presented in Figure 17.

Figure 16 indicates that the recovery time of the traditional ADRC for interference is 1.672 s, whereas that of the novel ADRC is 0.097 s. Figure 17 shows that the error of dy/dt and Z_{22} was removed completely at 0.435 and 2.865 s using the novel ADRC and traditional ADRC, respectively. Thus, the novel ADRC has shorter recovery and error removal times, weaker vibrations, and higher accuracy than the traditional ADRC.

Third, simulations are conducted when the speed of the motor suddenly changes. The initial motor speed is

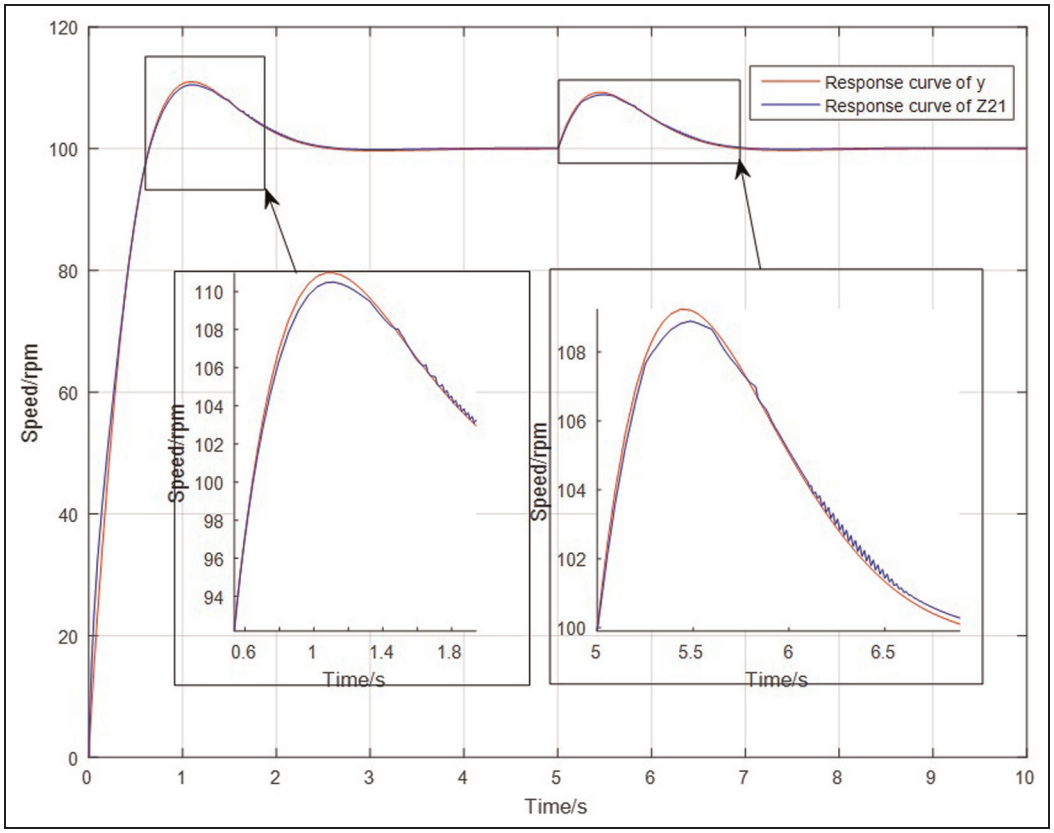

Figure 12. Response curves of y and Z_{21} with the traditional ADRC.

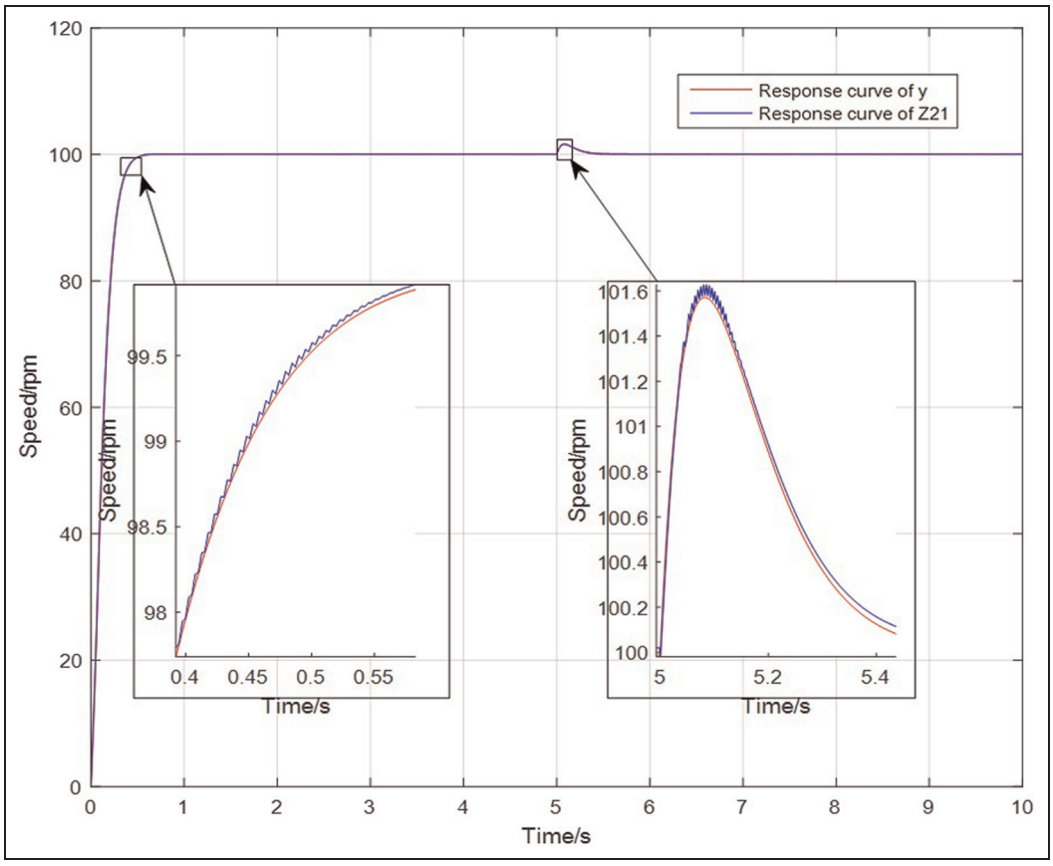

Figure 13. Response curves of y and Z_{21} with the novel ADRC.

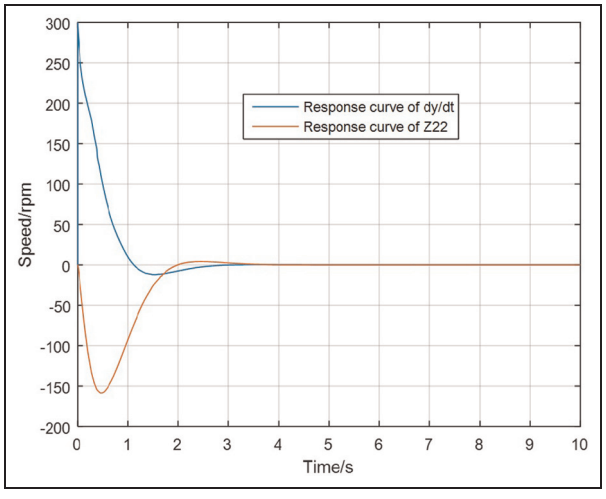

Figure 14. Response curves of dy/dt and Z_{22} with the traditional ADRC.

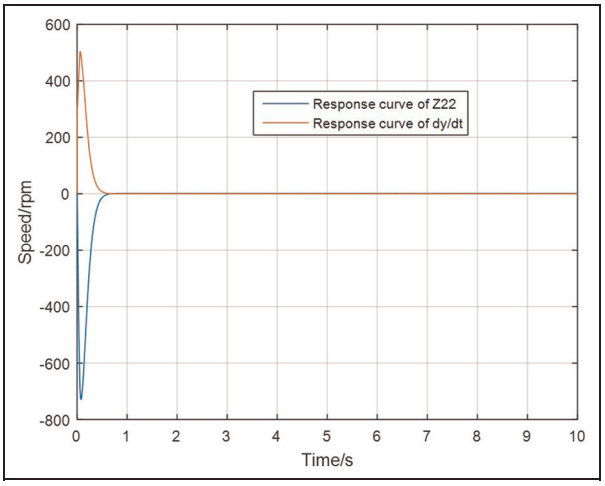

Figure 15. Response curves of dy/dt and Z_{22} with the novel ADRC.

100 r/min, which decreases to 50 r/min at 4 s. The speed response curves are shown in Figure 18. The figure indicates that the novel ADRC has smaller response curve fluctuations and better recovery capability than the traditional ADRC. The simulation results demonstrate that the amount of overshoot of the novel ADRC is 8.034% less than that of the traditional ADRC, and its response time is 1.588 s less than that of the traditional ADRC. The speed-loop parameters of overshoot amount and recovery time are presented in Table 4.

A random disturbance signal as measurement noise was applied on the traditional ADRC and novel

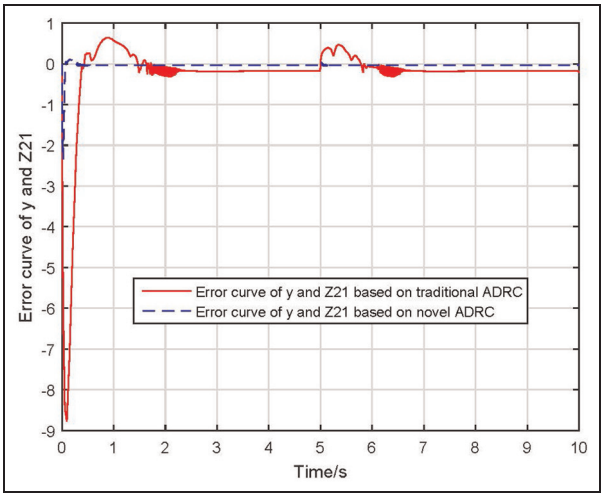

Figure 16. Response curves for the error of y and Z_{21}.

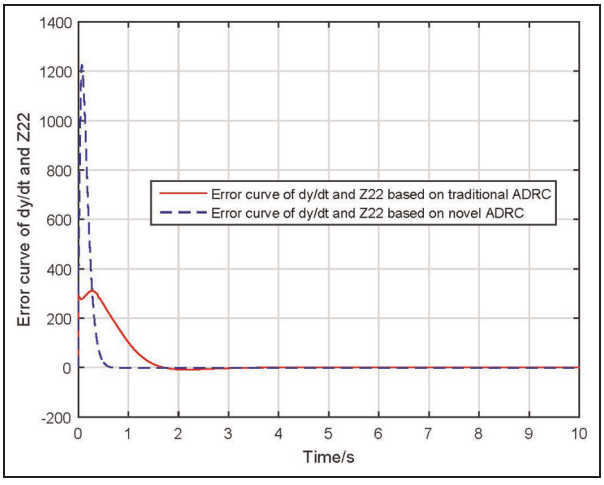

Figure 17. Response curves for the error of dy/dt and Z_{22}.

ADRC. Simulations were carried out and the outputs of ADRCs are shown in Figure 19. Figure 19 shows that the novel ADRC exhibits better elimination capacity for the measurement noise than the traditional ADRC.

Conclusion

In this study, a novel ADRC of the pitching axis speed loop for satellite cameras was introduced based on a new nonlinear function. The non-differentiable and discontinuous characters of the nonlinear function of the NLSEF of the traditional ADRC are addressed using the novel ADRC. The high-frequency flutter phenomenon is reduced significantly.

Simulations are performed when the motor starts without a load, an external load disturbance is suddenly applied on the motor, and the speed of the motor abruptly changes. The simulation results indicate that the system with the novel ADRC exhibits better dynamic performance, static performance, and robustness than the system with the traditional ADRC. The proposed design technique will be extended to the novel ADRC of the current loop and the position loop in our future study.

Table 4. System response parameters when the speed of the motor suddenly changes.

Strategy	Overshoot amount (%)	Recovery time (s)
Traditional ADRC	10.055	2.007
Novel ADRC	2.021	0.419

ADRC: active disturbance rejection controller.

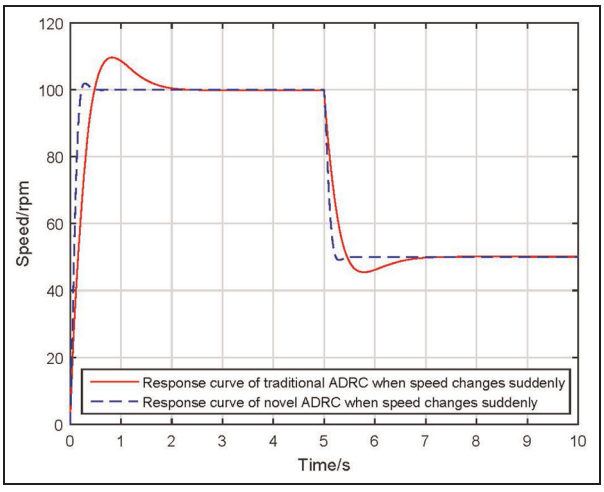

Figure 18. Speed response curves when the speed of the motor suddenly changes.

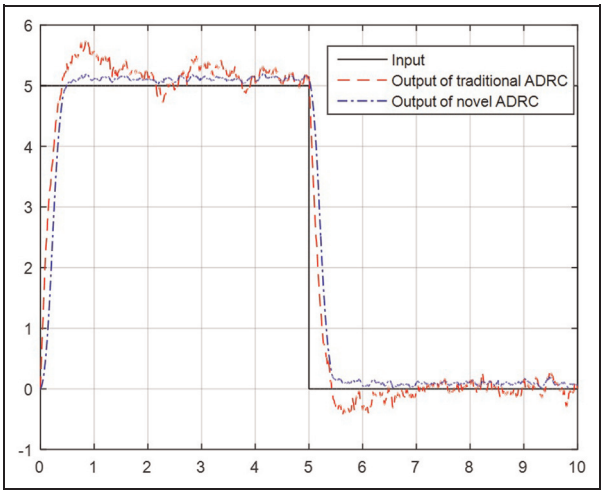

Figure 19. Outputs of traditional ADRC and novel ADRC with measurement noise.

Declaration of conflicting interests

The author(s) declared no potential conflicts of interest with respect to the research, authorship, and/or publication of this article.

Funding

The author(s) disclosed receipt of the following financial support for the research, authorship, and/or publication of this article: This work was supported by Key Project of Natural Science by Education Department of Anhui Province (KJ2015A316), Outstanding Young Talents at Home Visit the School Training Project (gxfxZD2016101), Natural Science Foundation of Anhui Province of China (1508085QE83), and Natural Science Foundation of China (51605464).

References

1. Guan X and Zheng GT. Integrated design of space telescope vibration isolation and attitude control. *J Astronaut* 2013; 34: 214–221.
2. Yang XB, Jiang L and Jing G. Image matching analysis and experiment of space borne camera swayed in the end of orbit life. *Chin J Space Sci* 2013; 33: 337–345.
3. Wang M, Cheng YF, Yang B, et al. On-orbit calibration approach for star cameras based on the iteration method with variable weights. *Appl Opt* 2015; 54: 6425–6432.
4. Han JQ. From PID to active disturbance rejection control. *IEEE T Ind Electron* 2009; 56: 900–906.
5. Guo BZ and Jin FF. The active disturbance rejection and sliding mode control approach to the stabilization of the Euler–Bernoulli beam equation with boundary input disturbance. *Automatica* 2013; 49: 2911–2918.
6. Xia Y, Shi P, Liu GP, et al. Active disturbance rejection control for uncertain multivariable systems with time-delay. *IET Control Theory A* 2007; 1: 75–81.
7. Stojadin M, ManojlovićŽarko P, et al. A novel active disturbance rejection based tracking design for laser system with quadrant photo detector. *Int J Control* 2015; 88: 1246–1256.
8. Zheng Q, Dong LL, Lee DH, et al. Active disturbance rejection control for MEMS gyroscopes. *IEEE T Contr Syst T* 2009; 17: 1432–1438.
9. Zhong Q, Zhang Y, Yang J, et al. Non-linear auto-disturbance rejection control of parallel active power filters. *IET Control Theory A* 2009; 3: 907–916.
10. Chong Y, Zhang K and Wang JY. Design and application of a servo control system based on a fuzzy active disturbance rejection control. *J Northwestern Polytech Univ* 2011; 29: 217–222.
11. Guo BZ and Liu JJ. Sliding mode control and active disturbance rejection control to the stabilization of one-dimensional Schrödinger equation subject to boundary control matched disturbance. *Int J Robust Nonlin* 2014; 24: 2194–2212.
12. Guo BZ and Jin FF. Sliding mode and active disturbance rejection control to stabilization of one-dimensional anti-stable wave equations subject to disturbance in boundary input. *IEEE T Automat Contr* 2013; 58: 1269–1274.
13. Guo BZ and Zhou HC. The active disturbance rejection control to stabilization for multi-dimensional wave equation with boundary control matched disturbance. *IEEE T Automat Contr* 2015; 60: 143–157.
14. Fu YL, Chen H, Liu HS, et al. Study on missile electro-hydraulic actuator system based on active disturbance rejection control method. *J Astronaut* 2012; 31: 1051–1055.
15. Xia YQ, Dai L, Fu M, et al. Application of active disturbance rejection control in tank gun control system. *J Franklin I* 2014; 351: 2299–2314.
16. Sira-Ramírez H, Linares-Flores J, García-Rodríguez C, et al. On the control of the permanent magnet synchronous motor: an active disturbance rejection control approach. *IEEE T Contr Syst T* 2014; 22: 2056–2063.
17. Zhu EL, Pang JF, Sun N, et al. Airship horizontal trajectory tracking control based on Active Disturbance Rejection Control (ADRC). *Nonlinear Dynam* 2014; 75: 725–734.
18. Gao ZQ. On the centrality of disturbance rejection in automatic control. *ISA T* 2014; 53: 850–857.
19. Huang Y and Xue WC. Active disturbance rejection control: methodology and theoretical analysis. *ISA T* 2014; 53: 963–976.
20. Wang YH, Yao Y and Ma KM. Analysis and application of Fal function filter. *Electr Mach Control* 2010; 14: 88–91.
21. Wu D and Chen K. Frequency-domain analysis of nonlinear active disturbance rejection control via the describing function method. *IEEE T Ind Electron* 2013; 60: 3906–3914.
22. Lin F, Sun H, Zheng QL, et al. Novel extended state observer for uncertain system with measurement noise. *J Contr Theor Appl* 2005; 22: 995–998.
23. Ran MP, Wang Q and Dong CY. Stabilization of a class of nonlinear systems with actuator saturation via active disturbance rejection control. *Automatica* 2016; 63: 302–310.
24. Xue WC, Bai WY, Yang S, et al. ADRC with adaptive extended state observer and its application to air–fuel ratio control in gasoline engines. *IEEE T Ind Electron* 2015; 62: 5847–5857.
25. Li JX, Xia Y, Qi X, et al. Absolute stability analysis of on-linear active disturbance rejection control for single-input–single-output systems via the circle criterion method. *IET Control Theory A* 2015; 9: 2320–2329.
26. Castaneda LA, Luviano-Juarez A and Chairez I. Robust trajectory tracking of a delta robot through adaptive active disturbance rejection control. *IEEE T Contr Syst T* 2015; 23: 1387–1398.
27. Qiu BB. *Research on improved active disturbance rejection control for hypersonic vehicle*. Harbin, China: Harbin Institute of Technology, 2014.
28. Li H, Shang JN, Chen Y, et al. The applications of nonlinear PI controller based on the Fal function in the DC-DC converter. *Trans China Electrotech Soc* 2014; 9: 326–331.
29. Liu YT, Kung TT, Chang KM, et al. Observer-based adaptive sliding mode control for pneumatic servo system. *Precis Eng* 2013; 37: 522–530.
30. Li R, Tong CN and Yang X. Active speed compensation method of direct torque control system and stability analysis. *Adv Mech Eng* 2015; 7: 1–11.